Motion of a Transverse/Parallel Grain Boundary in a Block Copolymer under Oscillatory Shear Flow

Zhi-Feng Huang, François Drolet, and Jorge Viñals*

School of Computational Science and Information Technology, Florida State University, Tallahassee, Florida 32306-4120

Received January 22, 2003; Revised Manuscript Received July 29, 2003

ABSTRACT: A mesoscopic model of a diblock copolymer is used to study the motion of a grain boundary separating two regions of perfectly ordered lamellar structures under an oscillatory but uniform shear flow. The case considered is a grain boundary separating lamellae along the so-called parallel orientation (with wavevector parallel to the velocity gradient direction) and along the transverse orientation (wavevector parallel to the shear direction). In the model considered, lamellae in the parallel orientation are marginal with respect to the shear, whereas transverse lamellae are uniformly compressed instead. A multiple scale expansion valid in the weak segregation regime and for low shear frequencies leads to a pair of envelope equations for the grain boundary. These equations show that the grain boundary moves by the action of the shear, with a net average velocity toward the transverse region. Three different dynamical effects are at play: a rigid deformation of the transverse region by the shear which increases its free energy, diffusive relaxation of the order parameter in the grain boundary region leading to relative phase motion between the two domains during a shear cycle, and wavenumber adjustment in the transverse region. We show that the average velocity of the boundary is an increasing function of shear frequency and that, except at very low frequencies, it can be expressed as the product of a mobility coefficient and a driving force given by the excess energy stored in the transverse phase being sheared.

1. Introduction

Self-assembly of block copolymers is one possible route to the development of nanostructured materials, either directly or as templates. The major challenge that needs to be overcome for widespread application of these materials is the development of long-ranged order in the polymer over scales much larger than the wavelength of the mesophase. The purpose of this paper is to investigate the motion of a grain boundary separating two lamellar regions oriented along different directions when the block copolymer is under an externally imposed, oscillatory shear flow. The study is motivated by the widespread use of both steady and oscillatory shear flows to induce long ranged order in lamellar phases.

The system under consideration is a symmetric diblock copolymer slightly below its order−disorder transition temperature T_{ODT} (weak segregation regime). The equilibrium phase is a lamellar structure in which nanometer-sized layers rich in A or B monomers alternate in space. When the copolymer is quenched from a high temperature to a temperature $T < T_{ODT}$, a transient but long-lived polycrystalline sample results comprised of an ensemble of locally ordered grains but of arbitrary orientations. A large number of defects are typically present in the sample including grain boundaries, dislocations, and disclinations.

Different methods of inducing macroscopic sample alignment are being investigated experimentally, including substrate-induced patterning,[1−3] step-mediated orientation of thin films,[4] electric fields that take advantage of a nonuniform dielectric constant[5,6] or of the existence of ions in the copolymer,[7] and oscillatory shear flows in bulk samples.[8−13] We focus here on the latter case for which there is no agreement at present on the issue of orientation selection as a function of the physical properties of the copolymer and the parameters of the flow. For the purposes of the discussion, three basic orientations of the lamellae relative to the shear flow are conventionally defined: parallel, in which the lamellar planes are parallel to the flow velocity; transverse, in which the lamellar normal is parallel to the flow; and perpendicular, in which the lamellar normal is parallel to the vorticity of the imposed flow. Recent reviews of experimental phenomenology can be found in refs 14 and 15. Briefly, two of the most widely studied diblock copolymers are poly(ethylene−propylene)−poly(ethylethylene) (PEP−PEE) and poly(styrene)−poly(isoprene) (PS−PI). In the case of PEP−PEE, parallel lamellae are observed at low shear rates, whereas the perpendicular orientation is observed at high frequencies.[9,10] It is possible to induce a transition from parallel to perpendicular by increasing the shear frequency, but the transformation does not appear to be reversible. The phenomenology described is just reversed for PS−PI: The perpendicular orientation is observed at low frequencies, while the parallel orientation is observed for high frequencies.[11,12] There is disagreement, however, in the low-frequency range depending on the preparation protocol of the sample, and the parallel orientation has also been observed in PS−PI in this limit.[13,16]

The effect of shear flows on lamellar alignment has also been investigated by numerical simulation. For steady shears, Zvelindovsky et al.[17] show that the shear is very effective in speeding up the formation of lamellar domains. In a two-dimensional system in which only parallel and transverse orientations are allowed, the shear ultimately leads to a perfectly aligned parallel sample. Any other orientation is eventually unstable against uniform melting. In three dimensions, on the other hand, lamellae are seen to form predominantly along the perpendicular direction. This qualitative result is consistent with earlier theoretical analyses by Cates and Milner,[18] and perhaps with Fredrickson's

10.1021/ma034083q CCC: $25.00 © 2003 American Chemical Society
Published on Web 11/19/2003

limit of high shear rate,[19] although it is not possible to make a definite comparison between in this case. However, the peak of the configuration structure factor remains quite broad, indicating the presence of a large number of defects. Ren et al.[20] have developed a cell dynamical system model to explicitly address oscillatory shears, albeit in two dimensions. They also show that the shear is very effective in speeding up the formation of lamellar domains and obtain the values of the necessary critical shear amplitude to attain complete sample alignment along the parallel direction. This critical amplitude decreases with the square of the shear frequency. The aspect ratio of the system (the ratio between its lateral dimension and the lamellar wavelength) is in the range 8−16 in both numerical studies, and therefore it was not possible to accommodate any extended defect in the simulations or any coexisting regions of different orientation as seen in the experiments.

In an attempt to clarify existing experimental phenomenology about orientation selection of lamellar phases, we considered a mesoscopic model of the block copolymer and undertook a stability analysis of the lamellar phase under oscillatory shear flows, with and without viscosity contrast between the microphases.[21,22] We found that there is a finite range of shear amplitudes within which periodic lamellar structures along a given direction exist. For amplitudes larger than a certain critical value, the lamellar phase "melts" into a disordered phase, possibly re-forming with a different orientation relative to the shear, the new orientation being within the band of allowed solutions. Lamellar configurations within the band of allowed solutions can in turn become unstable against long wavelength perturbations. The corresponding regions of instability were given in refs 21 and 22 as a function of the orientation of the lamellae and the shear rate. Broadly speaking, it was found that the region of stability of perpendicular lamellae is larger than that of parallel lamellae and both considerably larger than the region of stability of the transverse orientation. Our results also showed that the critical mode of instability is typically along the perpendicular orientation, so that the decay of an unstable region of parallel or transverse lamellae would lead, at least initially, to lamellae predominantly oriented along the perpendicular direction. These results were interpreted through a geometric description of the lamellar distortion, suggesting that the emerging mode of instability is the one that causes the largest decrease in lamellar wavelength under shear. Finally, the results were shown to be fairly insensitive to viscosity contrast between the microphases.

While the results just summarized narrow the range over which particular orientations can be in principle observed experimentally, they do not provide an orientation selection mechanism among competing, simultaneously stable stationary states. We therefore turn our attention to the competition between coexisting orientations in a macroscopic sample and to orientation selection mechanisms of dynamical nature. In addition, and in contrast with the two numerical studies alluded to earlier, we are primarily concerned with the extended system or large aspect ratio limit. Typical experiments in bulk melts, for example, easily involve aspect ratios of the order of 10^6, with configurations at long times and under shear exhibiting a distribution of regions with lamellae of different orientations separated by extended defects (see, e.g., refs 23 and 24).

While existing stability results limit the range of orientations that can be observed for a given quench depth and shear rate amplitude and frequency,[21,22] all three orientations (parallel, perpendicular, and transverse) remain linearly stable for moderate shear amplitudes and are indeed observed in experiments. Therefore, whether a single orientation will or will not be ultimately selected by the shear is expected to strongly depend on defect motion and, in particular, on the motion of fronts of boundaries separating regions of macroscopically distinct orientation. Our focus in this paper is on the motion of a boundary separating domains of parallel and transverse orientation because of the qualitatively different response of the two domains to the shear. Parallel lamellae in the mesoscopic description employed are marginal with respect to the shear and therefore unaffected by the flow. Transverse lamellae, on the other hand, are compressed by the shear, a fact that is shown to induce systematic boundary motion toward the region of transverse orientation in order to reduce the overall energy of the system. The shrinking of the transverse phase is a purely dynamical effect that cannot be accounted for by the stability analyses described above. Therefore, parallel lamellae are expected to become prevalent over transverse lamellae, even in those ranges of parameters of the polymer and of the flow in which transverse lamellae are linearly stable. This observation is not confined to microphase separation of diblock copolymers but is expected to hold as well in other systems of smectic symmetry in which a shear distortion couples to solidlike or elastic degrees of freedom on one side of a grain boundary, whereas the response of the other side is along the liquidlike direction.

Two important simplifications are introduced in our analysis: Viscosity contrast between the microphases is neglected, and the grain boundary is assumed to remain planar. The effect of viscosity contrast on the stability of a lamellar configuration was addressed in ref 22. Briefly, let $\mathbf{v} + \mathbf{u}$ be the actual flow field in the polymer, with $\mathbf{v}$ the imposed shear and $\mathbf{u}$ a correction (e.g., due to viscosity contrast). For perfectly ordered lamellae in an unbounded domain, fluid incompressibility leads to $\mathbf{q}\cdot\mathbf{u}_\mathbf{q} = 0$, where $\mathbf{q}$ is the lamellar wavevector. As a consequence, the flow field is parallel to the lines of constant monomer concentration ψ, and hence there is no advection of ψ due to the velocity field $\mathbf{u}$: $\mathbf{u}\cdot\nabla\psi = 0$. (The field $\mathbf{u}$ for the special case of a linear viscosity contrast is given explicitly in eq 13 of ref 22.) Therefore, only lamellar distortions away from planarity induce flows that couple back to the distortion, and this effect becomes of second order in the perturbation. Flows in the vicinity of a grain boundary of the type shown schematically in Figure 1 are expected to be more complex and to include a short wavelength component in region B that is probably damped and a long wavelength transverse component that could couple to transverse modulations of region A. The stability analysis of the planar boundary against modulation and including viscosity contrast between the microphases is beyond the scope of the current study. We simply argue below that even in the absence of viscosity contrast an oscillatory shear is sufficient to induce net motion of a planar boundary that would remain stationary otherwise.

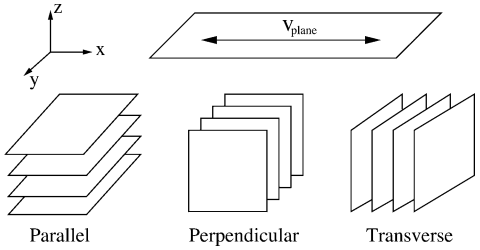

Figure 1. Schematic representation of the geometry considered including the shear direction and the three different lamellar orientations discussed in the text.

Grain boundary curvature also induces systematic motion in the absence of shear, as shown in ref 25. The local normal velocity of the boundary is asymptotically proportional to its mean curvature squared for a weakly curved boundary. If, as discussed above, a macroscopic sample contains an ensemble of differently oriented domains, a reduction in grain boundary surface area and structure coarsening occur. Although coarsening of a macroscopically isotropic lamellar phase has been addressed by a number of authors (see, e.g., ref 26 and references therein), little is known about the effect of shear. In the simpler case of a phase-separating binary, it is known that the shear flow competes with the coarsening process by elongating single phase domain and eventually leading to either their breakup or alignment with the flow (see, e.g., ref 27). A similar study of the effect of shear on lamellar phase coarsening has not, to our knowledge, been conducted.

2. Mesoscopic Model Equation of a Lamellar Phase under Shear

At a mesoscopic level, and for time scales that are long compared with the relaxation time of the polymer chain, a block copolymer melt is described by an order parameter $\psi(\mathbf{r})$ which represents the local density difference between the two monomers constituting the copolymer. The corresponding free energy was derived by Leibler in the weak segregation limit (close to T_{ODT})[28] and later extended by Ohta and Kawasaki to the strong segregation regime.[29] If the temporal evolution of ψ occurs through advection by a flow field as well as through local dissipation driven by free energy reduction, ψ obeys a time-dependent Ginzburg−Landau equation that in the symmetric case of equal volume fraction of the two monomers is given by[30]

$$\frac{\partial\psi}{\partial t} + \mathbf{v}\cdot\nabla\psi = \nabla^2(-\psi + \psi^3 - \nabla^2\psi) - B\psi \qquad (1)$$

All quantities have been made dimensionless, including the advection velocity $\mathbf{v}$ and the long-range polymer interaction coefficient B. The order−disorder transition between a disordered phase ($\psi = 0$) and a lamellar phase ($\psi \neq 0$) takes place at $B_0 = {}^1/_4$. For $B \gtrsim B_0$, ψ is a periodic function of wavenumber $q_0 = 1/\sqrt{2}$.

The physical system under consideration here is a layer of block copolymer, unbounded in the x and y directions, and being uniformly sheared along the z direction (Figure 1). The layer is confined between the stationary $z = 0$ plane, and the plane $z = d$ which is uniformly displaced parallel to itself with a velocity $\mathbf{v}_{plane} = \gamma d\omega \cos(\omega t)\hat{\mathbf{x}}$, where $\hat{\mathbf{x}}$ is the unit vector in the x direction.

We first briefly summarize the results of refs 21 and 22 concerning stationary lamellar solutions in shear flow. In the weak segregation limit $\epsilon = (B - B_0)/2B_0 \ll 1$, the solution for the monomer composition can be obtained perturbatively in ϵ

$$\psi(\mathbf{r}) = 2A(t)\cos(\mathbf{q}\cdot\mathbf{r}) + A_1(t)\cos(3\mathbf{q}\cdot\mathbf{r}) + \ldots \qquad (2)$$

where $A(t) \sim \mathcal{O}(\epsilon^{1/2})$ and $A_1(t)$ and higher order mode amplitudes are of higher order in ϵ. We have defined $\mathbf{r} = x_1\hat{\mathbf{x}} + x_2\hat{\mathbf{y}} + x_3(\gamma \sin(\omega t)\hat{\mathbf{x}} + \hat{\mathbf{z}})$, a vector that is expressed in a nonorthogonal basis set which follows the imposed shear, and $\mathbf{q} = (q_1, q_2, q_3)$, the wavevector in the corresponding reciprocal space basis set $\{\mathbf{g}_1 = \hat{\mathbf{x}} - \gamma \sin(\omega t)\hat{\mathbf{z}}, \mathbf{g}_2 = \hat{\mathbf{y}}, \mathbf{g}_3 = \hat{\mathbf{z}}\}$. Note that in this new coordinate system the wavevector of a perfectly ordered configuration is stationary. Three orientations relative to the shear can be defined as follows: $q_3 \neq 0$, $q_1 = q_2 = 0$ is a purely parallel orientation, $q_2 \neq 0$, $q_1 = q_3 = 0$ is a perpendicular orientation, and $q_1 \neq 0$, $q_2 = q_3 = 0$ is a transverse orientation.

For constant viscosity and if we neglect flow induced by the lamellae themselves, the velocity field in the layer is independent of monomer composition and is given by

$$\mathbf{v} = \gamma\omega \cos(\omega t) z\hat{\mathbf{x}} \qquad (3)$$

To lowest order in ϵ, the amplitude $A(t)$ satisfies the equation[21]

$$\frac{\mathrm{d}A}{\mathrm{d}t} = \sigma[q^2(t)]A - 3q^2(t)A^3 \qquad (4)$$

with $q^2(t) = q_1{}^2 + [\gamma \sin(\omega t)q_1 - q_3]^2 + q_2{}^2$ and $\sigma(q^2) = q^2 - q^4 - B$. This equation can be integrated to give the marginal stability boundaries and the function $A(t)$ itself.[21] From this analysis, a critical strain amplitude γ_c was identified, a function of the orientation $\mathbf{q}$ but independent of the frequency ω, such that for $\gamma < \gamma_c$ the uniform lamellar structure oscillates with the imposed shear, but for $\gamma > \gamma_c$ $A(t)$ decays to zero; i.e., the lamellar structure melts, according to the terminology used by experimentalists.

The stability of this base lamellar pattern was then addressed by Floquet analysis. Regions of stability were obtained for lamellar solutions of arbitrary orientation that were generally largest for orientations near the perpendicular direction and smallest in the vicinity of the transverse direction. As discussed in the Introduction, this stability analysis provides some guidance on the issue of orientation selection, but we wish to extend here the analysis of existence and stability to possible selection by dynamical mechanisms. The specific case considered in this paper is the motion of a grain boundary separating regions of uniform parallel and transverse orientations under oscillatory shear.

We use in what follows a different form of the equation governing the evolution of the monomer composition ψ, known as the Brazovski equation (or Swift−Hohenberg equation in the fluids literature).[18,19,31] Both this equation and eq 1 lead to the same amplitude or envelope equations near onset[32,33] and hence lead to identical results in the limit addressed in this paper. The Swift−Hohenberg equation for a dimensionless scalar order parameter is

$$\frac{\partial\psi}{\partial t} + \mathbf{v}\cdot\nabla\psi = \epsilon\psi - (\nabla^2 + q_0{}^2)^2\psi - \psi^3 \qquad (5)$$

Here all quantities have been made dimensionless with the introduction of a length scale $1/q_0$* and a time scale

$\tau_D = 1/Dq_0^{*2}$, where q_0^* is the critical wavenumber and D is the chain diffusivity of the copolymer. In the weak segregation limit $\epsilon \ll 1$. Assuming a system with a lamellar wavelength $\lambda_0^* \sim 300$ Å as for PEP−PEE-2[9] and a chain diffusivity $D \sim 10^{-11}$ cm^2/s close to T_{ODT} (= 96 °C) as estimated from the self-diffusion result of PEP−PEE-2,[34] we have $\tau_D \sim 0.03$ s. In this units, $q_0 = 1$ in eq 5, although we will retain the symbol q_0 in the equations that follow for clarity of presentation.

As was the case in the analyses presented in refs 21 and 22, we introduce a new frame of reference in which the velocity vanishes. In the case of an imposed oscillatory shear of amplitude γ and angular frequency ω, we define a set of nonorthogonal coordinates $x' = x - a(t)z$ and $z' = z$, where $a(t) = \gamma \sin(\omega t)$. We assume that the system is uniform in the third direction and therefore simply focus on a two-dimensional case. Equation 5 transforms to

$$\frac{\partial \psi}{\partial t} = \epsilon\psi - (\nabla'^2 + q_0^2)^2\psi - \psi^3 \tag{6}$$

where

$$\nabla'^2 = (1 + a(t)^2)\frac{\partial^2}{\partial x'^2} - 2a(t)\frac{\partial^2}{\partial x'\,\partial z'} + \frac{\partial^2}{\partial z'^2}$$

A solution of the linearization of eq 6 can be found by assuming

$$\psi(\mathbf{r}') = A\cos(\mathbf{q}\cdot\mathbf{r}')$$

Given that $(\nabla'^2 + q_0^2)\psi = (-q(t)^2 + q_0^2)\psi$ with $q(t)^2 = q_{x'}^2 + (a(t)q_{x'} - q_{z'})^2$, we find

$$\frac{dA}{dt} = \epsilon A - (-q(t)^2 + q_0^2)^2 A = \sigma(t)A \tag{7}$$

The disordered solution $A = 0$ becomes unstable when

$$\int_0^{2\pi/\omega} \sigma(t')\,dt' > 0$$

In analogy with the case analyzed in ref 21, we find several instability modes and associated thresholds:

(i) $q_{x'} = 0$, $q_{z'} = q_0$ $\quad \epsilon = 0$ parallel mode

(ii) $q_{z'} = 0$, $q_{x'} = \sqrt{\dfrac{4\gamma^2 + 8}{3\gamma^4 + 8\gamma^2 + 8}}\,q_0$

$$\epsilon = \frac{\gamma^4 q_0^4}{3\gamma^4 + 8\gamma^2 + 8}$$ transverse mode

(iii) $q_{x'} = \sqrt{\dfrac{2}{15\gamma^2 + 16}}\,q_0$, $q_{z'} = \sqrt{\dfrac{3\gamma^2 + 8}{15\gamma^2 + 16}}\,q_0$

$$\epsilon = \frac{8\gamma^2 q_0^4}{15\gamma^2 + 16}$$ mixed mode

3. Envelope Equations and Velocity of Motion for a Grain Boundary under Weak Shear

We focus on a special configuration comprising two perfectly ordered lamellar domains in a two-dimensional (2D) $x-z$ plane, initially oriented perpendicular to each other that meet at a grain boundary. We assume that both domains are initially of the same wavenumber q_0 at least far from the boundary, so that a planar grain boundary would be stationary in the absence of shear. We will neglect in this study any back flow induced by the lamellae themselves (through osmotic stresses), so that the velocity field **v** in eq 5 equals the imposed shear flow. A schematic representation of the configuration under study is shown in Figure 2. We denote by B the lamellae that lie parallel to the flow field and note that the order parameter ψ in this region is unaffected by the flow. Transverse lamellae are denoted by A. If the A lamellae were to adiabatically follow the imposed flow, both orientation and wavelength would be a periodic function of time as illustrated schematically in Figure 2. Because a local change in wavenumber away from q_0 always leads to a free energy increase in region A, while the free energy in region B remains unchanged, we anticipate grain boundary motion from region B to region A, thereby increasing the area occupied by parallel lamellae. Note that the study here is for the 2D system, but the results (including the direction and velocity of grain boundary motion) could be generalized to the three-dimensional transverse/perpendicular case.

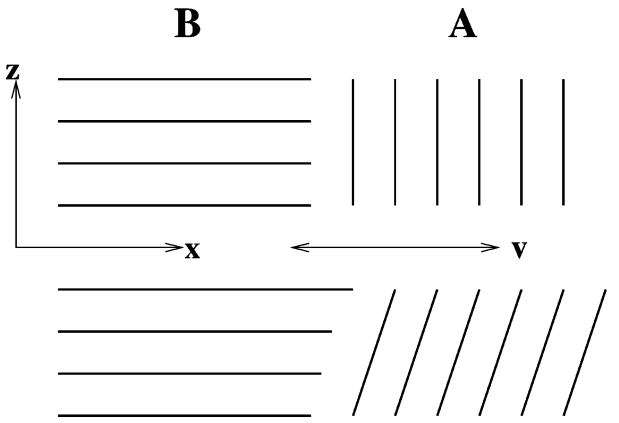

Figure 2. Schematic representation of a planar grain boundary that separates regions of parallel and transverse lamellae being uniformly sheared.

We first derive a set of amplitude (or envelope) equations from eq 6 by using a multiple scale approach. For $\epsilon \ll 1$, it is possible to extract the slow evolution of both lamellae and grain boundary by expanding the order parameter ψ in both regions around a periodic function, with amplitudes that are slowly varying in the grain boundary region (of very large extent in this limit). Our derivation follows closely that of Tesauro and Cross for the case of no flow,[35] and the details of our calculation are presented in the Appendix. The analysis is restricted to shears of small amplitude and low frequency. Specifically, and as seen in eq 7, consistency with the expansion in the weak segregation limit requires that $(-q(t)^2 + q_0^2)^2 \sim \mathcal{O}(\epsilon)$, a requirement that dictates the magnitude of the shear amplitude. Consider a system initially with a 90° grain boundary. In the transverse region A a small lamellar modulations would lead to a new wavenumber $q_{x'} \sim q_0 + \delta q_{x'}$ and $q_{z'} \sim \delta q_{z'}$, so that $-q(t)^2 + q_0^2 = q_0^2 a^2 + 2q_0\delta q_{x'} - 2q_0 a\delta q_{z'} + \delta q_{z'}^2$ + higher-order terms. Therefore, at lowest order and given that $-q(t)^2 + q_0^2$ has to remain $\mathcal{O}(\epsilon^{1/2})$, we have $a \sim \mathcal{O}(\epsilon^{1/4})$, $\delta q_{x'} \sim \mathcal{O}(\epsilon^{1/2})$, and $\delta q_{z'} \sim \mathcal{O}(\epsilon^{1/4})$. This means that the time-dependent rotation of the grain boundary with respect to the initial 90° orientation is small (due to the small shear amplitude $\gamma \sim \mathcal{O}(\epsilon^{1/4})$ and $a = \gamma \sin(\omega t)$). The slow length scales in the multiple scale analysis can now be chosen as $X = \epsilon^{1/2}x'$ and $Z = \epsilon^{1/4}z'$.

A similar procedure in region B yields $q_{x'} \sim \delta q_{x'}$ and $q_{z'} \sim q_0 + \delta q_{z'}$. Hence $-q(t)^2 + q_0^2 = -2q_0 a\delta q_{x'} + \delta q_{x'}^2 + 2q_0\delta q_{z'} + ...$, leading to $\delta q_{x'} \sim \mathcal{O}(\epsilon^{1/4})$, $\delta q_{z'} \sim \mathcal{O}(\epsilon^{1/2})$, and again $a \sim \mathcal{O}(\epsilon^{1/4})$. Thus, we choose as slow length scales in region B $\bar{X} = \epsilon^{1/4}x'$ and $\bar{Z} = \epsilon^{1/2}z'$.

In addition to the slow spatial scales defined above, we also introduce a slow time (or small frequency) scale $T = \epsilon t$. In addition, we also have to satisfy the requirement that the dimensional angular frequency $\omega^* < \omega_c$, the angular frequency at which chain relaxation effects become relevant. For PEE-PEP-2 for example, $\omega_c \simeq 1.0$ s^{-1} already at 40 °C[9] and is much larger closer to T_{ODT}. In practice, we have used $\omega = 0.005-0.1$ corresponding to $\omega^* \sim 0.2-4$ s^{-1}.

From the multiple scale analysis given in the Appendix, the order parameter ψ can be written as the superposition of two modes in the x' and z' directions, i.e., $\psi = [A \exp(iq_0x') + B \exp(iq_0z')]/\sqrt{3}$, and to $\mathcal{O}(\epsilon^{3/2})$, the complex amplitudes A and B satisfy the equations

$$\partial_t A = \{\epsilon - [2iq_0(\partial_{x'} - a\partial_{z'}) + \partial_{z'}^2 - q_0^2a^2]^2\}A - |A|^2A - 2|B|^2A \quad (8)$$

$$\partial_t B = \{\epsilon - [2iq_0(\partial_{z'} - a\partial_{x'}) + \partial_{x'}^2]^2\}B - |B|^2B - 2|A|^2B \quad (9)$$

At this order, there are two kinds of contributions to these amplitude equations arising from the shear. One is proportional to derivatives of the amplitudes (in particular $a\partial_{x'}$) and is nonzero only in the grain boundary region. It describes variations of the amplitude of the lamellae due to the changing orientation of the grain boundary with respect to the lamellar planes and incorporates local diffusive relaxation of the order parameter at the grain boundary. The second contribution arises from the term $q_0^2a^2$ in eq 8. It does not contain any spatial derivative and therefore is important in the entire bulk A region. This term leads to a change in the amplitude A as it is advected by the flow. The corresponding change in the free energy of region A does not average to zero over a period and leads to net motion of the grain boundary.

We have numerically solved the coupled, two-dimensional complex equations (8) and (9) for $\epsilon = 0.04$, $q_0 = 1$, $\gamma = 0.3$, and a variety of shear frequencies ω. In the calculations, region B is surrounded by two identical domains of transverse A lamellae so that periodic boundary conditions in both x' and z' can be used. The equations are integrated with a pseudo-spectral algorithm in which the linear terms are treated with the Crank−Nicholson scheme for time stepping and the nonlinear terms with a second-order Adams−Bashford scheme. We used a computational domain of size 512 × 512, a grid spacing $\Delta x' = \Delta z' = \lambda_0/8$ (with $\lambda_0 = 2\pi/q_0$), and a time interval $\Delta t = 0.1$. Stationary solutions obtained in the absence of shear provide the initial conditions for A and B.

The instantaneous location of the grain boundary $x'_{gb}(t)$ is implicitly defined by $\langle|B(x'_{gb})|\rangle_{z'} = \epsilon/4$ (with $\langle\cdots\rangle_{z'}$ denoting the average over z') and its velocity v_{gb} as the rate of change of x'_{gb}. Figure 3 shows v_{gb} as a function of t/τ for $\omega = 0.1$ and 0.01, with $\tau = 2\pi/\omega$ the period of the applied shear. Positive (negative) values of v_{gb} indicate motion toward region A (B). Following an initial transient, the velocity oscillates in time with an amplitude that increases with ω. The temporal

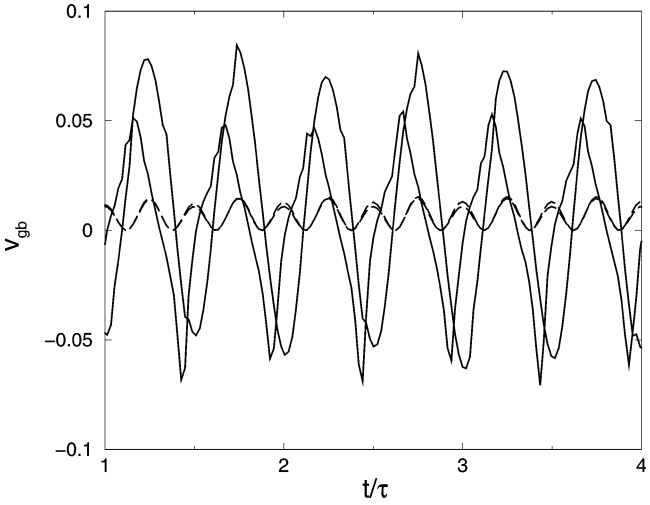

Figure 3. Grain boundary velocity as a function of time obtained by numerical solution of eqs 8 and 9. Two different angular frequencies are shown (solid curves, in order of decreasing amplitude): $\omega = 0.1$ and 0.01. Also shown is the analytic approximation of eq 16 calculated at the same angular frequencies (dashed curves). The other parameters are $\gamma = 0.3$, $\epsilon = 0.04$, and $q_0 = 1$.

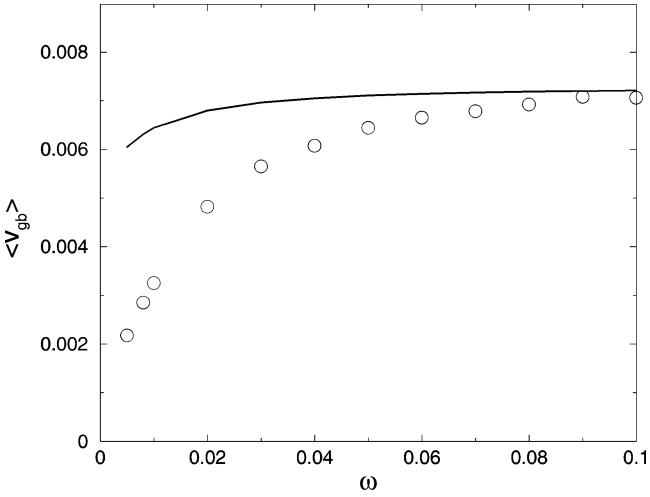

Figure 4. Temporal average of the grain boundary velocity (over a period τ) as a function of the angular frequency of the shear, with $\gamma = 0.3$, $\epsilon = 0.04$, and $q_0 = 1$. The symbols correspond to the time average of the velocities numerically obtained from eqs 8 and 9, and the solid line is the time average of the approximative velocity given in eq 16. The results are averaged between $t = 10\tau$ and 20τ.

average of the velocity is positive; i.e., motion is directed toward domain A. This can be seen more clearly in Figure 4, which shows $\langle v_{gb}\rangle = (1/\tau)\int_0^\tau v_{gb}(t)\,dt$ for different angular frequencies ω. We find that the average speed of the boundary increases with the shear frequency ω at low ω and then tends to saturate for larger frequencies.

The motion of the grain boundary shown in Figure 3 can be understood as the combination of a rigid distortion of the lamellae due to the local shear and the concomitant diffusive relaxation of the order parameter. Diffusive relaxation at the boundary involves breakup of transverse A lamellae during the first part of the shear cycle, followed by reconnection in the latter part of the cycle during which the shear velocity is negative. The breakup/reconnection process is more pronounced at low frequencies, leading to the smaller velocity amplitude at $\omega = 0.01$ compared to $\omega = 0.1$, as shown

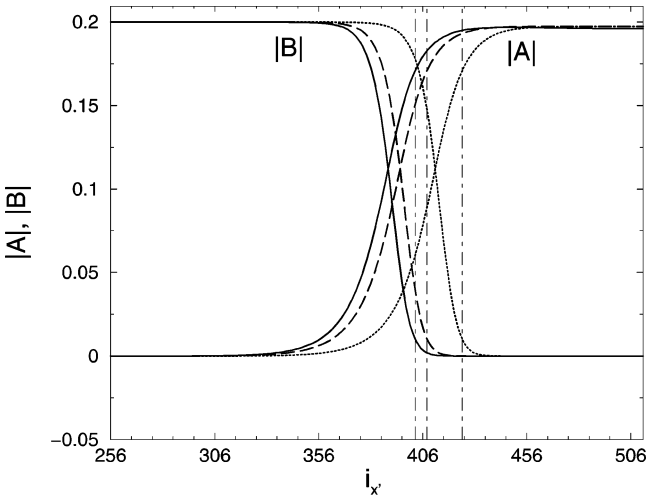

Figure 5. Profile of moduli $|A|$ and $|B|$ with respect to grid position $i_{x'}$ along the x' direction, at fixed z' $i_{z'} = L_{z'}/2 = 512/2$, at different times $t = 10\tau$ (solid lines), 20τ (dashed lines), and 50τ (dotted lines) for $\omega = 0.1$. The other parameters are the same as in Figures 3 and 4. The instantaneous boundary positions $x'_{gb}(t)$ are indicated by the vertical dot−dashed lines (from left to right: $t = 10\tau$, 20τ, and 50τ).

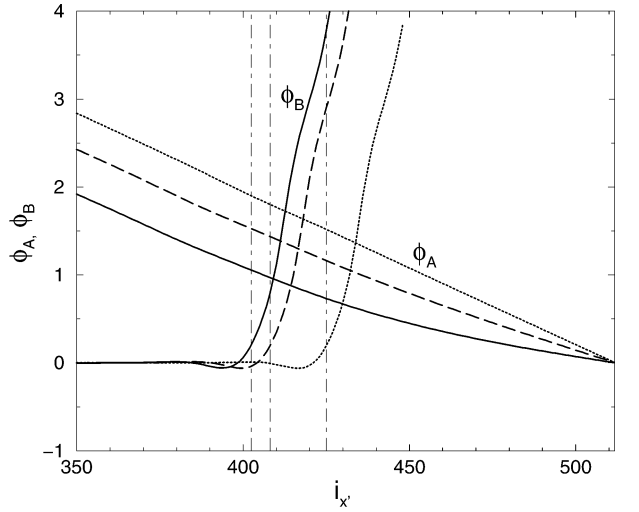

Figure 6. Phases ϕ_A and ϕ_B of the amplitudes A and B as a function of grid position $i_{x'}$ along the x' direction. As in Figure 5, solid lines correspond to time $t = 10\tau$, dashed lines to $t = 20\tau$, and dotted lines to $t = 50\tau$. The other parameters as well as the boundary positions (vertical dot−dashed lines) are the same as in Figure 5. Note that only the phases of not too small amplitudes (e.g., both real and imaginary parts of A and B are larger than 10^{-5}) are calculated and shown here.

in Figure 3. The interfacial relaxation is primarily a phase mode that is captured with the complex amplitudes A and B.

The local oscillation of A and B in the boundary region also leads to an unexpected wavenumber shift of the A lamellae in this region, which eventually propagates into the bulk. We show in Figures 5 and 6 the profiles of the modulus and phase of A and B, $A = |A| \exp(i\phi_A)$ and $B = |B| \exp(i\phi_B)$, for $\omega = 0.1$ and times $t = 10\tau$, 20τ, and 50τ. Figure 5 shows that far from the grain boundary the moduli approach a constant value while near the boundary $|A|$ ($|B|$) smoothly decays to zero from the transverse (parallel) region to the parallel (transverse) region, as expected. Figure 5 also shows the values of x'_{gb} for the same times (vertical dot−dashed lines). On the other hand, the spatial dependence of the phases ϕ_A and ϕ_B at $t = 10\tau$, 20τ, and 50τ is illustrated in Figure 6. The phase of transverse lamellae A ϕ_A becomes linear in x' near the grain boundary, i.e., $\phi_A \propto -\delta q \cdot x'$, with $\delta q > 0$ ($\delta q \simeq 0.017/\Delta x'$ for the parameters used in the figure). The region of linearity increases with time. This indicates a readjustment of the local wavenumber of region A at the boundary which progressively diffuses into the bulk. The phase ϕ_B remains zero in the entire B region. In summary, the imposed shear flow leads to oscillatory motion of the boundary with a nonzero averaged front velocity toward the transverse A domain and to transverse lamellae expansion (or wavenumber compression) in the sheared frame.

To isolate any possible transient effects on boundary motion due to the observed wavenumber compression in region A, we have modified the initial condition used in our numerical integration by defining

$$A(x', z', t) = A'(x', z', t)e^{-i\delta q \cdot x'} \tag{10}$$

so that the bulk of region A is always occupied by transverse lamellae of wavenumber $q_0 - \delta q$. Given eq 10, we transform the envelope equations (8) and (9) to

$$\partial_t A' = \{\epsilon - [2iq_0(\partial_{x'} - a\partial_{z'}) + \partial_{z'}{}^2 - (-2q_0\delta q + q_0{}^2a^2)]^2\}A' - |A'|^2A' - 2|B|^2A' \tag{11}$$

and

$$\partial_t B = \{\epsilon - [2iq_0(\partial_{z'} - a\partial_{x'}) + \partial_{x'}{}^2]^2\}B - |B|^2B - 2|A'|^2B \tag{12}$$

The initial condition involves one domain of B surrounded by two domains of A so that periodic boundary conditions in both x' and z' can be used. We also have A' uniform at $t = 0$ in domain A, so that the wavenumber of the bulk transverse lamellae is $q_0 - \delta q$. No large-scale phase motion in region A is expected in this case.

The results for the grain boundary velocity v_{gb} and the spatial profiles of $|A'|$ and $|B|$ obtained from direct numerical solution of the transformed equations (11) and (12) are virtually identical to those in Figures 3−5. The spatial profiles of $\phi_{A'}$ and ϕ_B are plotted in Figure 7 with $\delta q = 0.017/\Delta x'$. $\phi_B(x')$ remains the same as in Figure 6, while $\phi_{A'}$ now adopts the form of a uniformly translating front.

The propagating solutions shown in Figures 5 and 7 suggest expressions of the form (in the sheared frame)

$$A'(x', z', t) \simeq A'^s(x' - x'_{gb}(t), z'; a) \quad \text{and} \quad B(x', z', t) \simeq B^s(x' - x'_{gb}(t), z'; a) \tag{13}$$

where A'^s and B^s are stationary solutions of eqs 11 and 12 (with the boundary conditions given), which formally depend on the parameter a. This latter dependence results from the dependence of the stationary amplitude profiles A'^s and B^s on the instantaneous state of shear of the system given by the parameter a. Then $(\partial_t A', \partial_t B) \simeq -v_{gb}(\partial_{\tilde{x}} A'^s, \partial_{\tilde{x}} B^s)$ where we have introduced the notation $\tilde{x} = x' - x'_{gb}$. Following ref 36, we multiply eq 11 by $\partial_{\tilde{x}} \bar{A}'^s$ and eq 12 by $\partial_{\tilde{x}} \bar{B}^s$ (with $\bar{A}'^s$ and $\bar{B}^s$ the complex conjugate of A'^s and B^s, respectively), add the

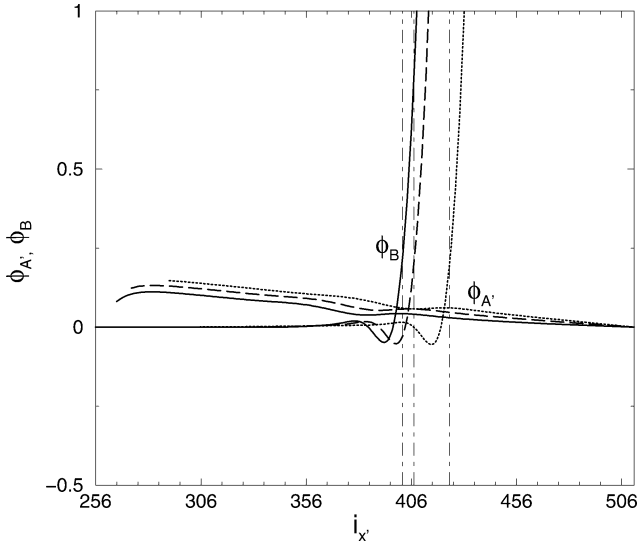

Figure 7. Phases $\phi_{A'}$ of the transformed amplitude A' (by $A = A' \exp(-i\delta q \cdot x')$ with $\delta q = 0.017/\Delta x'$) as well as ϕ_B of amplitude B as a function of grid position $i_{x'}$, for different times $t = 10\tau$ (solid lines), 20τ (dashed lines), and 50τ (dotted lines). All the other parameters are the same as Figure 6.

two equations, and integrate over $\tilde{x}$ and z' to obtain

$$2v_{gb}\int_0^d dz' \int_{-\infty}^{+\infty} d\tilde{x}\, (|\partial_{\tilde{x}} A'^s|^2 + |\partial_{\tilde{x}} B^s|^2) = \int_0^d dz' \,[\mathscr{F}(+\infty) - \mathscr{F}(-\infty)] \quad (14)$$

where $\mathscr{F}(\pm\infty) = \mathscr{F}(\tilde{x} \to \pm\infty, z')$ and

$$\mathscr{F}(\tilde{x}, z') = -\epsilon(|A'^s|^2 + |B^s|^2) + \frac{1}{2}(|A'^s|^4 + |B^s|^4) + 2|A'^s|^2|B^s|^2 + |[2iq_0(\partial_{\tilde{x}} - a\partial_{z'}) + \partial_{z'}{}^2 - (-2q_0\delta q + q_0{}^2a^2)]A'^s|^2 + |[2iq_0(\partial_{z'} - a\partial_{\tilde{x}}) + \partial_{\tilde{x}}{}^2]B^s|^2 \quad (15)$$

is the free energy density associated with eqs 11 and 12. The integral on the left-hand side of eq 14 is time-dependent, playing a role similar to an inverse mobility or friction coefficient, whereas the right-hand side represents the effective driving force for grain boundary motion. It equals the free energy increase upon shearing relative to the planar, unsheared boundary and can be evaluated by using the values $|A'^s(-\infty)| = 0$, $|B^s(-\infty)| = \sqrt{\epsilon}$, and $|B^s(+\infty)| = 0$. Also, when $t \gg 1$, we have $|A'^s| \approx [\epsilon - (-2q_0\delta q + q_0^2a^2)^2]^{1/2}$ from eq 11. As a result, $\mathscr{F}(-\infty) = -\epsilon^2/2$, $\mathscr{F}(+\infty) = -[\epsilon - (-2q_0\delta q + q_0{}^2a^2)^2]^2/2$, and therefore

$$v_{gb} = \frac{(-2q_0\delta q + q_0{}^2\gamma^2 \sin^2(\omega t))^2[2\epsilon - (-2q_0\delta q + q_0{}^2\gamma^2 \sin^2(\omega t))^2]}{4\int_0^d dz' \int_{-\infty}^{+\infty} d\tilde{x}\, (|\partial_{\tilde{x}} A'^s|^2 + |\partial_{\tilde{x}} B^s|^2)/d} \quad (16)$$

For $\delta q = 0$, the driving force in the numerator scales as ϵ^2, whereas the inverse mobility in the denominator approximately scales as $\epsilon^{3/2}$. Hence, the average velocity of the boundary vanishes with $\epsilon^{1/2}$.[37]

We compare this analytic result with the numerical integration of the governing equations in Figures 3 and 4. To evaluate the denominator of eq 16, we obtain $A'(x', z', t)$ and $B(x', z', t)$ from the numerical integration of eqs 11 and 12. The apparent mobility coefficient also oscillates in time, but with a steady average value after a sufficiently long time. If, following previous work without shear,[25,33,36] we were to use A instead of A' in (13), the apparent mobility coefficient decays to zero as the width of the apparent boundary (i.e., the region with large-scale phase motion of transverse lamellae and then the nonzero gradient of amplitude A) increases without bound.

The average velocity $\langle v_{gb} \rangle$ calculated from the approximate expression (16) is shown in Figure 4. It only shows a weak dependence on ω. The driving force $\mathscr{F}(+\infty) - \mathscr{F}(-\infty)$ is independent of ω for very low frequencies and increases only marginally at larger frequencies. As a result, variations in $\langle v_{gb} \rangle$ with ω arise solely from small changes in the denominator of eq 16. In contrast, the numerical values of $\langle v_{gb} \rangle$ also shown in Figure 4 exhibit a pronounced decrease as ω approaches zero. This discrepancy can be understood by noting that in order to obtain eq 16 the order parameter ψ (or the amplitudes A' and B) has been assumed to adiabatically follow the shear in eq 13 by considering the stationary solutions of (11) and (12). While the adiabatic approximation works well in the absence of shear,[25,33] and while the boundary region appears to be well described by a propagating front solution, the phase difference between the boundary velocity and the imposed shear (see, e.g., solid curve in Figure 3) indicates the important role of local diffusive relaxation at low shear frequencies. This effect is absent in the assumption (13) and hence in the corresponding velocity (16).

It is difficult to unambiguously determine the response of the grain boundary in the static limit of $\omega \to 0$. On one hand, the analytic approximation (16) yields a nonzero value of the average velocity $\langle v_{gb} \rangle$ if $\delta q \neq 0$. For as long as the wavenumber of region A remains or is maintained away from q_0, there will remain a free energy imbalance between the A and B domains, and a net boundary velocity would be expected. On the other hand, eq 16 becomes less accurate at low frequencies as diffusive relaxation becomes prevalent (Figure 4). It is therefore possible that the wavenumber of region A would decay back to q_0 and with it the boundary velocity to zero.

4. Discussion

In the absence of shear ($\gamma = 0$), and following a quench of the diblock copolymer from an initially disordered configuration at $T > T_{ODT}$ to a final temperature below T_{ODT}, initial composition fluctuations are amplified exponentially, with a growth rate that is isotropic. Lamellar regions emerge and coarsen as a function of time. Coarsening rates and the role of topological defects in a two-dimensional system have been discussed in ref 26. To our knowledge, a similar investigation in three dimensions has not been carried out. If the quench takes place under shear, the mean-field instability threshold depends on orientation, as shown in ref 21. The first threshold is to a mixed parallel-perpendicular mode at $B_c = {}^1/_4$, followed by a bifurcation to a transverse mode at $B_c = {}^1/_4 - \gamma^4/32 + \mathcal{O}(\gamma^6)$, and to a parallel-transverse mode at $B_c = {}^1/_4 - \gamma^2/8 + \mathcal{O}(\gamma^4)$. Therefore, for shallow quenches fluctuations along different orientations would be amplified at different rates, leading to predominantly parallel and perpendicular oriented domains even from an isotropic initial condition. Thermal fluctuations, on the other hand, are known to significantly modify these

conclusions.[18,19,38,39] In particular, thermal fluctuations render the mean-field supercritical bifurcation a weakly subcritical bifurcation, with a transition temperature that increases with γ. In any event, the distribution of orientations following a quench in shear flow is expected not to be isotropic.

Regardless of whether the copolymer is quenched in shear flow or not, a macroscopically disordered configuration will result at intermediate times comprising regions of well-saturated monomer composition, but with a wide distribution of lamellar orientations. The distribution of observable orientations is reduced by the shear, as those orientations that are unstable against long wavelength perturbations will quickly decay when the monomer composition locally reaches nonlinear saturation. Insofar the melt is Newtonian at the low shear frequencies investigated in refs 21 and 22, one would expect lamellae that are predominantly perpendicular, and to a lesser degree parallel, with small projections of the lamellar wavevector on the transverse direction. There also exists a small region of stable transverse lamellae. Further structure coarsening under shear will involve an initially anisotropic distribution of orientations and hence is expected to be qualitatively different from the isotropic case. In metals, for example, coarsening of an initially anisotropic distribution of orientations leads to texture.[40]

The results of this paper further indicate that regions where parallel and transverse lamellae meet will move, even when both parallel and transverse lamellae are linearly stable. The net motion of the grain boundary is driven by free energy reduction because parallel lamellae are unaffected by the shear, whereas transverse lamellae are elastically compressed, a compression that leads to an increase in energy that is relieved through boundary motion. Also, the effect of local diffusion and relaxation near the grain boundary plays an important role on the detailed behavior of the boundary motion, including the backward motion of grain boundary (negative boundary velocity), the expansion of transverse lamellae in sheared frame, and the phase shift of velocity for small shear frequency. The upper bound to the average velocity of grain boundary motion is given by the analytic approximation (16) as some of the driving force presented there is dissipated away through local diffusive relaxation in the boundary region. Since a similar argument can be made for a boundary separating perpendicular and transverse lamellae, we would expect that regions of a macroscopic sample oriented along any combination of parallel and perpendicular orientations will grow at the expense of any remaining transverse lamellae.

If viscous or viscoelastic contrast between the microphases is allowed, a secondary flow appears which is orientation-dependent.[19,22] The velocity field of this secondary flow is parallel to the lamellar planes (assuming incompressibility) and largest for a uniform parallel configuration, while it vanishes for a uniform perpendicular configuration. This flow is weak in the weak segregation limit and has negligible consequences on the stability of a lamellar configuration against long wavelength perturbations.[22] However, its possible effect on boundary motion has not been investigated yet.

Acknowledgment. This research has been supported by the National Science Foundation under Contract DMR-0100903.

Appendix: Derivation of Amplitude Equations and the Related Asymptotic Behavior

We describe in this Appendix the derivation of the amplitude (or envelope) equations (8) and (9). The lamellar system we study is shown schematically in Figure 2, with a grain boundary and an imposed oscillatory shear flow. From the discussion of section 3, the slowly varying amplitude of the mode $e^{iq_0x'}$ in the sheared frame has characteristic length scales $X = \epsilon^{1/2}x'$ and $Z = \epsilon^{1/4}z'$, while the mode $e^{iq_0z'}$ has characteristic scales $\bar{X} = \epsilon^{1/4}x'$ and $\bar{Z} = \epsilon^{1/2}z'$. Also, a weak shear is considered, namely, $a = \gamma \sin(\omega t) \sim \mathcal{O}(\epsilon^{1/4})$.

The operator $(\nabla'^2 + q_0^2)^2$ can now be expanded in powers of ϵ as

$$(\nabla'^2 + q_0^2)^2 = L_0^2 + \epsilon^{1/4}(2L_0L_1) + \epsilon^{1/2}(L_1^2 + 2L_0L_2) + \epsilon^{3/4}(2L_0L_3 + 2L_1L_2) + \epsilon(2L_0L_4 + 2L_1L_3 + L_2^2) \quad \text{(A.1)}$$

with

$$L_0 = \partial_{x'}^2 + \partial_{z'}^2 + q_0^2$$

$$L_1 = 2(\partial_{x'}\partial_{\bar{X}} + \partial_{z'}\partial_Z - \bar{a}\partial_{x'}\partial_{z'})$$

$$L_2 = \partial_{\bar{X}}^2 + \partial_Z^2 + 2(\partial_{x'}\partial_X + \partial_{z'}\partial_{\bar{Z}} - \bar{a}\partial_{z'}\partial_{\bar{X}} - \bar{a}\partial_{x'}\partial_Z) + \bar{a}^2\partial_{x'}^2$$

$$L_3 = 2[\partial_{\bar{X}}\partial_X + \partial_Z\partial_{\bar{Z}} - \bar{a}(\partial_{z'}\partial_X + \partial_{x'}\partial_{\bar{Z}} + \partial_{\bar{X}}\partial_Z) + \bar{a}^2\partial_{x'}\partial_{\bar{X}}]$$

$$L_4 = \partial^2_X + \partial_{\bar{Z}}^2 - 2\bar{a}(\partial_X\partial_Z + \partial_{\bar{X}}\partial_{\bar{Z}}) + \bar{a}^2(2\partial_{x'}\partial_X + \partial^2_{\bar{X}})$$

with $\bar{a}$ defined by $a = \epsilon^{1/4}\bar{a}$. We also expand ψ as

$$\psi = \epsilon^{1/2}\psi_0 + \epsilon\psi_1 + \epsilon^{3/2}\psi_2 + \ldots \quad \text{(A.2)}$$

and assume that both the frequency of the imposed shear and the associated variation of ψ is over a slow time scale $T = \epsilon t$. From eqs 6, A.1, and A.2, we obtain at $\mathcal{O}(\epsilon^{1/2})$ the equation

$$-L_0^2\psi_0 = 0 \quad \text{(A.3)}$$

which admits the solution

$$\psi_0 = \frac{1}{\sqrt{3}}[A_0e^{iq_0x'} + B_0e^{iq_0z'} + \text{c.c.}] \quad \text{(A.4)}$$

with A_0 and B_0 functions of X, Z, $\bar{X}$, $\bar{Z}$, and T. At $\mathcal{O}(\epsilon)$, eq 6 reduces to

$$-L_0^2\psi_1 = L_1^2\psi_0 \quad \text{(A.5)}$$

where we have used the fact that $L_0\psi_0 = 0$, and taken advantage that the cross derivative term $a\partial_{x'}\partial_{z'}$ vanishes when acting on ψ_0, so that the solution at this order is also time independent (in the sheared frame of reference). Since ψ_0 is an eigenmode of L_0 with zero eigenvalue, the right-hand side of eq A.5 must vanish in order for it to admit a solution. Solvability requires that the scalar product $\langle\psi_0^+|L_1^2\psi_0\rangle = 0$; that is, the right-hand side of eq A.5 must be orthogonal to the zero eigenfunctions of the adjoint of L_0. But $\langle\psi_0^+|L_1^2\psi_0\rangle = \langle L_1^+\psi_0^+|L_1\psi_0\rangle = ||L_1\psi_0||^2 = 0$, from which it follows $L_1\psi_0 = 0$. As a result of this solvability condition, A_0 and B_0

must be independent of $\bar{X}$ and Z, respectively. Equation A.5 then reduces to eq A.3 and $\psi_1 = [A_1 e^{iq_0 x'} + B_1 e^{iq_0 z'} + \text{c.c.}]/\sqrt{3}$.

Finally, at $\mathcal{O}(\epsilon^{3/2})$, the multiple scale analysis yields the equation

$$L_0{}^2\psi_2 = -\partial_T\psi_0 + \psi_0 - \psi_0{}^3 - (2L_0L_4 + 2L_1L_3 + L_2{}^2)\psi_0 - (2L_0L_2 + L_1{}^2)\psi_1 \quad \text{(A.6)}$$

Again, the functions ψ_0 and ψ_1 are zero eigenmodes of the operator L_0, so that the projections of the terms on the right-hand side of eq A.6 on these eigenfunctions must vanish. From this condition, we obtain the following amplitude equations

$$\partial_T A_0 = \{1 - [2iq_0(\partial_X - \bar{a}\partial_Z) + \partial_Z{}^2 - q_0{}^2\bar{a}^2]^2 - |A_0|^2 - 2|B_0|^2\}A_0 \quad \text{(A.7)}$$

and

$$\partial_T B_0 = \{1 - [2iq_0(\partial_{\bar{Z}} - \bar{a}\partial_{\bar{X}}) + \partial^2_{\bar{X}}]^2 - |B_0|^2 - 2|A_0|^2\}B_0 \quad \text{(A.8)}$$

where we have used the fact that $L_0\psi_0 = L_1\psi_0 = 0$ and have set $L_1{}^2\psi_1 = 0$. The set of equations (A.7) and (A.8) governs the evolution of the slowly varying envelopes of the base lamellar pattern, including variations both in the direction parallel and perpendicular to the grain boundary. In the absence of shear ($\bar{a} = 0$), these two equations reduce to the case studied by Manneville and Pomeau[36] and by Tesauro and Cross.[35]

We return now to unscaled variables

$$\psi = \frac{1}{\sqrt{3}}[A(x', z', t)e^{iq_0x'} + B(x', z', t)e^{iq_0z'} + \text{c.c.}] \quad \text{(A.9)}$$

so that the two complex amplitudes $A = \epsilon^{1/2}A_0$ and $B = \epsilon^{1/2}B_0$ obey the coupled equations

$$\partial_t A = \{\epsilon - [2iq_0(\partial_{x'} - a\partial_{z'}) + \partial_{z'}{}^2 - q_0{}^2a^2]^2 - |A|^2 - 2|B|^2\}A \quad \text{(A.10)}$$

and

$$\partial_t B = \{\epsilon - [2iq_0(\partial_{z'} - a\partial_{x'}) + \partial_{x'}{}^2]^2 - |B|^2 - 2|A|^2\}B \quad \text{(A.11)}$$

as transformed from eqs A.7 and A.8. This is one of the main results of our calculation and is given in eqs 8 and 9.

The amplitude equations (A.10) and (A.11) need to be supplemented with appropriate boundary conditions. First we have that $A(x' \to -\infty, z', t) = 0$ and $B(x' \to +\infty, z', t) = 0$. Furthermore, at large distances from the grain boundary inside domain B, $|B| = \sqrt{\epsilon}$, independent of the flow parameters. By contrast, the amplitude A inside domain A satisfies the equation $\partial_t|A| = (\epsilon - q_0{}^4a^4)|A| - |A|^3$ in the limit $x' \to +\infty$. This equation admits the solution

$$|A(+\infty, t)| = \{e^{-f(t)}[2\int_0^t e^{f(t')}\,dt' + |A(+\infty, 0)|^{-2}]\}^{-1/2} \quad \text{(A.12)}$$

where $f(t) = (2\epsilon - {}^3/_4q_0{}^4\gamma^4)t + q_0{}^4\gamma^4[(\sin 2\omega t)/2\omega - (\sin 4\omega t)/16\omega]$. The asymptotic behavior of eq A.12 at large times changes qualitatively with the sign of the constant $2\epsilon - {}^3/_4q_0{}^4\gamma^4$. When this constant is negative, the prefactor $e^{-f(t)}$ diverges exponentially with time and $|A(+\infty, t)|$ decays to zero. If, on the other hand, $2\epsilon - {}^3/_4q_0{}^4\gamma^4 > 0$, Laplace's method can be used to approximate the integral in the expression for $|A|$, which reduces to a periodic function

$$|A(+\infty, t)| = \left\{\sqrt{\frac{\pi}{g(t)}}e^{h^2(t)/4g(t)}\,\text{erfc}\left[\frac{h(t)}{2\sqrt{g(t)}}\right]\right\}^{-1/2} \quad \text{(A.13)}$$

where $g(t) = \omega q_0{}^4\gamma^4(\sin 2\omega t - {}^1/_2 \sin 4\omega t)$ and $h(t) = 2\epsilon + q_0{}^4\gamma^4(\cos 2\omega t - {}^1/_4 \cos 4\omega t - {}^3/_4)$. The condition $2\epsilon - {}^3/_4q_0{}^4\gamma^4 = 0$ which separates these two cases can be understood in terms of a maximum strain amplitude $\gamma^* = (8\epsilon/3q_0{}^4)^{1/4}$ above which the lamellar phase of domain A will melt. Note that γ^* is independent of the shear frequency ω.

References and Notes

(1) Fasolka, M.; Harris, D.; Mayes, A.; Yoon, M.; Mochrie, S. G. *Phys. Rev. Lett.* **1997**, *79*, 3018.
(2) Rockford, L.; Liu, Y.; Mansky, P.; Russell, T.; Yoon, M.; Mochrie, S. *Phys. Rev. Lett.* **1999**, *82*, 2602.
(3) Fasolka, M.; Hayes, A. *Annu. Rev. Mater. Sci.* **2001**, *31*, 323.
(4) Segalman, R.; Yokoyama, H.; Kramer, E. *Adv. Mater.* **2001**, *13*, 1152.
(5) Amundson, K.; Helfand, E.; Quan, X.; Smith, S. *Macromolecules* **1993**, *26*, 2698.
(6) Amundson, K.; Helfand, E.; Quan, X.; Hudson, S.; Smith, S. *Macromolecules* **1994**, *27*, 6559.
(7) Tsori, Y.; Tournilhac, F.; Leibler, L. arXiv:cond-mat/0301116.
(8) Hadziioannou, G.; Mathis, A.; Skoulios, A. *Colloid Polym. Sci.* **1979**, *257*, 136.
(9) Koppi, K.; Tirrell, M.; Bates, F.; Almdal, K.; Colby, R. *J. Phys. II* **1992**, *2*, 1941.
(10) Koppi, K.; Tirrel, M.; Bates, F. *Phys. Rev. Lett.* **1993**, *70*, 1449.
(11) Patel, S.; Larson, R.; Winey, K.; Watanabe, H. *Macromolecules* **1995**, *28*, 4313.
(12) Gupta, V.; Krishnamoorti, R.; Kornfield, J.; Smith, S. *Macromolecules* **1995**, *28*, 4464.
(13) Leist, H.; Maring, D.; Thurn-Albrecht, T.; Wiesner, U. *J. Chem. Phys.* **1999**, *110*, 8225.
(14) Hamley, I. *The Physics of Block Copolymers*; Oxford University Press: New York, 1998.
(15) Larson, R. G. *The Structure and Rheology of Complex Fluids*; Oxford University Press: New York, 1999.
(16) Maring, D.; Wiesner, U. *Macromolecules* **1997**, *30*, 660.
(17) Zvelindovsky, A.; Sevink, G.; van Vlimmeren, B.; Maurits, N.; Fraaije, J. *Phys. Rev. E* **1998**, *57*, R4879.
(18) Cates, M.; Milner, S. *Phys. Rev. Lett.* **1989**, *62*, 1856.
(19) Fredrickson, G. *J. Rheol.* **1994**, *38*, 1045.
(20) Ren, S.; Hamley, I.; Teixeira, P.; Olmsted, P. *Phys. Rev. E* **2001**, *63*, 041503.
(21) Drolet, F.; Chen, P.; Viñals, J. *Macromolecules* **1999**, *32*, 8603.
(22) Chen, P.; Viñals, J. *Macromolecules* **2002**, *35*, 4183.
(23) Polis, D.; Winey, K. *Macromolecules* **1998**, *31*, 3617.
(24) Qiao, L.; Winey, K.; Morse, D. *Macromolecules* **2001**, *34*, 7858.
(25) Boyer, D.; Viñals, J. *Phys. Rev. E* **2001**, *63*, 061704.
(26) Boyer, D.; Viñals, J. *Phys. Rev. E* **2001**, *64*, 050101(R).
(27) Frischknecht, A. *Phys. Rev. E* **1998**, *58*, 3495.
(28) Leibler, L. *Macromolecules* **1980**, *13*, 1602.
(29) Ohta, T.; Kawasaki, K. *Macromolecules* **1986**, *19*, 2621.
(30) Oono, Y.; Bahiana, M. *Phys. Rev. Lett.* **1988**, *61*, 1109.
(31) Swift, J.; Hohenberg, P. *Phys. Rev. A* **1977**, *15*, 319.
(32) Shiwa, Y. *Phys. Lett. A* **1997**, *228*, 279.
(33) Boyer, D.; Viñals, J. *Phys. Rev. E* **2002**, *65*, 046119.
(34) Dalvi, M.; Lodge, T. *Macromolecules* **1994**, *27*, 3487.
(35) Tesauro, G.; Cross, M. *Philos. Mag. A* **1987**, *56*, 703.
(36) Manneville, P.; Pomeau, Y. *Philos. Mag. A* **1983**, *48*, 607.
(37) Just as a reference, recall that the excess energy of the boundary per unit length scales as $\epsilon^{3/2}$.
(38) Bates, F.; Fredrickson, G. *Annu. Rev. Phys. Chem.* **1990**, *41*, 525.
(39) Hohenberg, P.; Swift, J. *Phys. Rev. E* **1995**, *52*, 1828.
(40) Mullins, W.; Viñals, J. *Acta Metall. Mater.* **1993**, *41*, 1359.

MA034083Q